DISPERSION ENGINEERING WITH LEAKY-MODE RESONANCE STRUCTURES

By

XIN WANG

Presented to the Faculty of the Graduate School of
The University of Texas at Arlington in Partial Fulfillment
of the Requirements
for the Degree of

MASTER OF SCIENCE IN ELECTRICAL ENGINEERING

THE UNIVERSITY OF TEXAS AT ARLINGTON
May 2010

ACKNOWLEDGEMENTS

I wish to express my deepest gratitude to my supervising professor, Dr. Robert Magnusson, for his highly competent guidance and persistent support during the past three years of my education. I am also grateful to Dr. Mehrdad Shokooh-Saremi for his support, encouragement and pertinent advice. Furthermore, I would like to thank my graduate committee members Dr. Kambiz Alavi, Dr. Weidong Zhou and Dr. Mingyu Lu for their help and valuable comments.

I have been fortunate to work in an excellent group of graduate students from whom I have learned a lot and with whom I have fruitfully collaborated on a number of research projects. Among them I am very grateful to Kyu Lee for his kind training on nano-fabrication fundamentals and constant help, and Dr. Yiwu Ding for our collaboration on the analysis of periodic devices.

My education in optics and photonics has begun at Harbin Institute of Technology, Harbin, China, in the Optoelectronics Laboratory led by Dr. Deying Chen, to whom I wish to express my sincere appreciation. I would also like to thank my teacher Dr. Yuanqin Xia for his help in the experiments and my undergraduate thesis.

April 15, 2010

ABSTRACT

DISPERSION ENGINEERING WITH LEAKY-MODE

RESONANCE STRUCTURES

Xin Wang, M.S.

The University of Texas at Arlington, 2010

Supervising Professor: Robert Magnusson

In the thesis, a numerical method for the analysis of optical pulses propagation through leaky-mode/guided-mode resonance (GMR) structures is implemented by integrating a Fourier decomposition technique and the rigorous coupled-wave analysis (RCWA) method. Dispersion properties of several GMR structures such as single-grating-layer GMR filters, coupled GMR filters, and cascaded GMR filters are studied and their interaction with optical pulses investigated. For device applications, a high-Q transmission filter is formed by coupling GMR reflection filters which can withstand typical attenuation in silicon. Wavelength division multiplexing (WDM) filters are proposed by cascading a number of GMR transmission filters. Generally, a N channel DWDM filter can be realized by cascading N+1 GMR transmission filters. The channel bandwidth in this structure is sensitive to the gap width between the two neighboring GMR filters. Both the channel bandwidth and channel spacing are inversely proportional to the number of cascaded GMR filters for a given gap width. For slow light applications, a conceptual optical delay line device with desired time delay and flat-dispersion is proposed by treating double GMR transmission filters as a cavity and then cascading such cavities.

TABLE OF CONTENTS

LIST OF ILLUSTRATIONS

Figure Page

LIST OF TABLES

CHAPTER 1

INTRODUCTION

1.1 Dispersion Types

In optics, dispersion is a phenomenon in which each spectral component of an optical pulse propagates with a slightly different group velocity, resulting in pulse broadening in time. Dispersion is one of the key factors limiting the transmission bandwidth in today's optical communication systems. Generally, dispersion effects are discussed in the context of pulse propagation over a long distance within a waveguide (most commonly, an optical fiber). However, with recent advances toward ultrahigh-bandwidth transmission and shorter pulses being used, dispersion issues become increasingly significant, even for propagation over short distances. There are five principal sources of dispersion: modal dispersion, material dispersion, waveguide dispersion, polarization-mode dispersion and nonlinear dispersion [1]. In most cases, pulse broadening results from the combined contributions of these effects, although they are not strictly additive.

In multimode fibers, modal dispersion occurs due to the different group velocities of various modes. The pulse broadening arising from modal dispersion is roughly proportional to the fiber length. Material dispersion occurs in a dispersive medium which has a wavelength (or frequency) dependent refractive index $n(\lambda)$. The group velocity of an optical pulse travelling through such a medium is defined by $v_g = c_0/N$, where $N = n-\lambda_0 dn/d\lambda_0$ (c_0 and λ_0 are the vacuum speed and wavelength of light, respectively) is called the group index. The corresponding material dispersion coefficient D_λ is [1]

$$D_\lambda = - (\lambda_0/ c_0)(d^2n/d \lambda_0^2). \qquad (1.1)$$

It is called normal dispersion when D_λ is negative, meaning that the spectral components of longer wavelengths travel faster than those of shorter wavelengths [1]. If D_λ is positive, we call it anomalous dispersion, meaning that spectral components of longer wavelengths travel slower than those of shorter wavelengths. Waveguide dispersion, in essence, is the dependence of the group velocity on the wavelength for each mode in the waveguide [1]. Polarization mode dispersion is a special case of modal dispersion, where two different polarizations (TE and TM) of light travel at different velocities due to the random imperfections and asymmetries of waveguides. When light intensity in a waveguide is so high that the refractive index becomes intensity dependent, the waveguide will exhibit nonlinear dispersion.

This thesis primarily deals with waveguide dispersion, which is also referred to as chromatic dispersion (CD) to emphasize the wavelength dependence, or group-velocity dispersion (GVD) to emphasize the role of group velocity, because this type of dispersion occurs in optical fibers, which are most commonly used in today's telecommunication systems. GVD is one of the most important limiting factors determining the data rate that can be transported through a single-mode fiber. In general, for a waveguide mode with an angular frequency ω and a propagation constant β, the group velocity dispersion is defined as [1]

$$GVD = - (2\pi c_0/\lambda^2)(d^2\beta/d\omega^2) = (2\pi c_0/\lambda^2 v_g^2)(dv_g/d\omega), \qquad (1.2)$$

where $\lambda = 2\pi c_0/\omega$ is the vacuum wavelength and $v_g = d\omega/d\beta$ is the group velocity.

1.2 Dispersion Engineering

Since waveguide dispersion limits the performance of single-mode fibers, more advanced fiber designs aim at reducing this effect by using special refractive-index profiles to alter the chromatic dispersion characteristics. Dispersion-shifted fibers (DSF) [2] have been successfully fabricated by using a linearly tapered core refractive index and a reduced core radius; this type of fiber can shift the zero-chromatic dispersion wavelength from 1.3 μm to 1.55

μm, where the fiber has its lowest attenuation. Dispersion-flattened fibers have been implemented by using a quadruple-clad layered grading. Dispersion-compensating fiber (DCF) [3] has a reversed dispersion coefficient compared with that of a conventional fiber. In addition, dispersion management and control in modern communication systems have motivated various research efforts toward development of dispersion management techniques and devices, such as chirped Bragg gratings [4]. Dispersion can also be controlled by use of an achromatic Fourier transformer [5]. Another technique is cascading a number of all-pass filters to attain a desired group velocity delay [6-8]. A summary of various dispersion management techniques can be found in [9].

Leaky-mode (or guided-mode) resonance occurs when the incident wave is coupled with a guided mode supported by a periodically-modulated dielectric medium under phase matching conditions. The amplitude-based spectral properties of resonant leaky-mode elements have been intensively studied both numerically and experimentally due to their unique properties and functionalities. Plenty of work has been performed in the aspects of diffraction efficiency, device applications, design, simulation and fabrication. The external spectral resonance signatures can have complex shapes with high efficiency in both reflection and transmission [10-18]. It has been shown that subwavelength periodic leaky-mode waveguide films with one-dimensional periodicity provide diverse spectral characteristics such that even single-layer elements can function as narrow-line bandpass filters, polarized wideband reflectors, wideband polarizers, polarization-independent elements, and wideband antireflection films [19-20]. The spectra can be further engineered with additional layers [21-22]. The relevant physical properties of these elements can be explained in terms of the structure of the second (leaky) photonic stopband and its relation to the symmetry of the periodic profile [23]. The interaction dynamics of the leaky modes at resonance contribute to sculpting the spectral bands. The leaky-mode spectral placement, their spectral density, and their levels of interaction

strongly affect device operation and functionality [19]. Thus, there has been a considerable amount of research performed on the spectral attributes of these elements.

In contrast, little work has been done to investigate the temporal responses of such nanostructures or their interaction with optical short pulses until recently [24-31]. Schreier et al. treated a sinusoidally-modulated waveguide grating at oblique incidence, computing the phase variation of the reflectance near resonance relative to modulation strength. They quantified the degree to which the structural parameters control the amount of delay achievable with computed values of delay ranging from sub-ps to ~40 ps depending on conditions [24-25]. Using a finite-difference time-domain (FDTD) computational approach, Mirotznik et al. evaluated the temporal response of a subwavelength dielectric grating that was designed previously [26] as a reflection-type GMR element. The model input pulse was Gaussian with center wavelength of 510 nm, spectral width of 5000 nm, and temporal pulse width of ~5 fs. They noted that the reflected energy persisted for ~1 ps after the incident field decayed [27]. Later, Suh et al. designed a 2D photonic-crystal-slab-type GMR transmission filter computing the resonance amplitude, transmission spectrum, and group delay. For a 1.2 μm thick slab, a peak delay of about 10 ps was obtained at 1550 nm; the spectral width of the response was ~0.8 nm [28]. Nakagawa et al. presented a method to model ultra-short optical pulse propagation in periodic structures, based on the combination of Fourier spectrum decomposition and rigorous coupled-wave analysis (RCWA) [29]. They simulated an incident pulse (167 fs) on a resonant grating supporting two modes and found that two pulses were transmitted with shapes similar to the excitation pulse shape. Vallius et al. modeled spatial and temporal pulse deformations generated by GMR filters. They illuminated the structure with a Gaussian temporal pulse of 2 ps duration centered at 633 nm wavelength. Lateral spread and temporal decompression were observed in the reflected and transmitted pulses [30]. As the spectrum of the pulse was not well accommodated by the GMR element, the reflection efficiency of the pulse was relatively low.

Ichikawa et al also presented an analysis method for femtosecond-order optical pulses diffracted by periodic structure based on FDTD [31-32].

This thesis will address the introduction of dispersion engineering with leaky-mode resonance structures. Moreover, by cascading a number of single-grating-layer GMR filters, we find device applications of dispersion properties of leaky-mode resonance structures in optical delay lines, GMR filters with high Q-factor, dense wavelength division multiplexing (DWDM) filters, and slow light techniques. Specifically, Chapter 2 discusses the numerical formalism and dispersion engineering with one-dimensional leaky-mode resonance structures. Coupled leaky-mode resonance reflection filters can provide tunable sensitivity, time delay, and attain high Q-factors. Transmission filters with a desired time delay and flat dispersion are realizable by cascading a number of identical leaky-mode resonance transmission elements. Chapter 3 deals with the various practical applications of dispersion characteristics of leaky-mode resonance structures including GMR filters with high Q-factor, DWDM filters and slow light element. A summary of the thesis and conclusions is the content of Chapter 4.

CHAPTER 2

ONE-DIMENSIONAL LEAKY-MODE RESONANCE STRUCTURES

2.1 Time Delay and Dispersion

A leaky waveguide mode can be represented by a pole in the complex propagation constant ($\gamma = \beta + j\alpha$) plane. For a waveguide grating structure with a periodicity of Λ, the field solutions are Bloch waves represented by complex poles with separation of $2\pi/\Lambda$ in the real axis β (i.e. $\beta = \beta_0 + m2\pi/\Lambda$, here β_0 is the propagation constant for the fundamental TE_0 mode and can be calculated from planar waveguide dispersion relation; m is the wave number). The magnitude of the imaginary part α is the radiation coefficient (leakage) [17]. The complex reflection amplitude is given by

$$r = \eta/(k-(\beta + j\alpha)), \qquad (2.1)$$

where η is a constant related to the coupling strength between the incident wave and guided mode field in the waveguide, $k = n_c 2\pi \sin\theta/\lambda$ is the tangential incident wave vector and θ is the incident angle. When the coupling relation $k = \beta$ is satisfied, a leaky-mode resonance occurs due to the excitation and rescattering of a leaky mode in the waveguide. For a zero-order resonant leaky-mode structure, only zero-order diffraction field can propagate through the structure and all higher orders are cutoff, meaning the propagation constant is

$$\beta = \beta_0 - 2\pi/\Lambda. \qquad (2.2)$$

The group delay and dispersion are derived from the phase of the complex reflection amplitude [33]. Specifically, if we denote $\phi = \arg(r)$ as the phase of reflection coefficient and expand ϕ in a Taylor series about the resonance frequency ω_0, the first derivative $d\phi/d\omega$ is considered as a measure of the group delay τ; the dispersion D is essentially the rate of change of delay with wavelength, so we obtain

$$\tau = d\phi/d\omega = -\lambda^2/(2\pi c)\, d\phi/d\lambda \qquad (2.3)$$

$$D = d\tau/d\lambda. \qquad (2.4)$$

2.2 Numerical Formalism

Let's consider a transform-limited, TE-polarized Gaussian pulse as represented by the following equation

$$E_y(t) = E_0 \exp[-\frac{(t-t_0)^2}{T^2}]\exp[j\omega_0(t-t_0)], \qquad (2.5)$$

where E_0 is the amplitude of the pulse; T is the temporal pulse width ($T = \sigma (2\ln 2)^{-1/2}$; σ is the full width at half maximum (FWHM) of the $|E_y(t)|^2$); t_0 is the offset of the pulse peak; $\omega_0 = 2\pi c_0/\lambda_0$ is the central angular frequency; c_0 and λ_0 are the speed of light and central wavelength in vacuum respectively [30-32, 34].

To use rigorous coupled-wave analysis method (RCWA), such a Gaussian pulse has to be decomposed into its monochromatic Fourier components (plane waves), which is performed by the Fourier transform and proper discretization. The corresponding Gaussian continuous spectrum of the given pulse is given by

$$E_y(\omega) = \sqrt{\pi} E_0 T \exp[-\frac{(\omega-\omega_0)^2}{(2/T)^2}]\exp[-j\omega t_0]. \qquad (2.6)$$

In numerical simulation, this continuous spectrum is discretized by imposing a finite bandwidth $\Delta\omega = 2M\delta\omega$ centered at ω_0, where δω is frequency sampling rate. Thus, the incident pulse is represented by a finite number (2M+1) of discrete frequency components at frequencies $\omega_n = \omega_0 + n\delta\omega$ (where n = {-M,…,0,…,M}). The cutoff frequencies of the bandwidth are $\omega_c = \omega_0 \pm M\delta\omega$ [29]. These discrete monochromatic components are then treated independently by the well-established RCWA analysis technique, which, at a given incident angle, provides the complex reflection coefficients $R(\omega_n)$ (or $R(\lambda_n)$) and complex transmission coefficients $T(\omega_n)$ (or $T(\lambda_n)$) of every diffraction orders. In addition, the independent analysis of each monochromatic component can facilitate the inclusion of material dispersion effects. The

reflected pulse $E_R(\omega_n)$ and transmitted pulse $E_T(\omega_n)$ in frequency-domain for a specific diffraction order are thus respectively given by the following two equations:

$$E_R(\omega_n) = E_y(\omega_n)R(\omega_n)\,, \quad (2.7)$$

$$E_T(\omega_n) = E_y(\omega_n)T(\omega_n)\,. \quad (2.8)$$

To obtain the time-domain representation of the reflected and transmitted pulses, the standard inverse Fourier transform is performed. Since the frequency domain representation of the fields is discrete and finite, Riemann sum can substitute the integral in the inverse Fourier transform. In other words, the reflected and transmitted fields can be obtained by superimposing the resulting spectral components, as is given by Eq. (2.9) and Eq. (2.10), assuming that the Fourier kernel is included in the expression for the fields $E_R(t; \omega_n)$ and $E_T(t; \omega_n)$ [29].

$$E_R(t) = \frac{1}{2\pi}\int_{-\infty}^{\infty} E_R(\omega)\exp(j\omega t)d\omega = \frac{1}{2\pi}\sum_n E_R(t;\omega_n)\delta\omega\,, \quad (2.9)$$

$$E_T(t) = \frac{1}{2\pi}\int_{-\infty}^{\infty} E_T(\omega)\exp(j\omega t)d\omega = \frac{1}{2\pi}\sum_n E_T(t;\omega_n)\delta\omega\,. \quad (2.10)$$

Figure 2.1 clarifies the flow of this computational method. Utilizing this technique, we find the time delay of the pulse as well as incident, reflected, and transmitted pulse shapes over a wide range of incident pulse widths (from ~several fs to hundreds of ps). The time delay (τ) and delay dispersion (D) for transmission elements are calculated as

$$\tau = (\lambda^2/2\pi c)\,d\varphi/d\lambda \quad (2.11)$$

$$D = -d\tau/d\lambda\,. \quad (2.12)$$

where φ is the wavelength (λ) dependent phase in transmission [32,35-36]. Note that for reflection elements, the sign change of time delay (τ) and delay dispersion (D) should be placed.

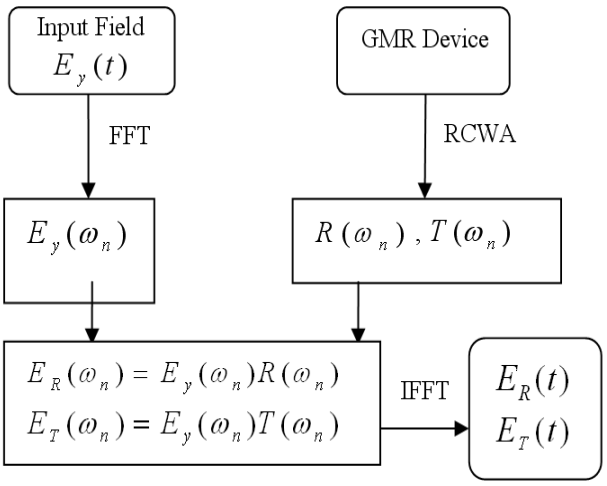

Figure 2.1 Flow chart of the computational procedure utilized to obtain the output pulse shapes in wavelength and time domains. FFT: Fast Fourier Transform, RCWA: Rigorous Coupled-Wave Analysis, and IFFT: Inverse Fast Fourier Transform.

2.3 Simulation Results

The results presented in this thesis are calculated by combining the Fourier decomposition techniques and RCWA method. Details about the formalization and implementation of RCWA method can be found in references [35-36]. Some of the structures are designed with the particle swarm optimization (PSO) technique [37-38].

2.3.1 Single-grating-layer GMR Structures

Figure 2.2 illustrates a typical single-grating-layer leaky-mode resonant structure. A four-parts grating layer with high-index n_{si} (silicon) and low-index 1.0 (air) is sandwiched between two semi-infinite media: cover region and substrate region. The cover region is usually assumed as air and the substrate region is taken as glass with a refractive index of n_s = 1.48. The average refractive index of the grating layer has to be higher than the substrate and cover refractive indices for wave guiding and leaky-mode resonances to occur. Filling factors F_1, F_3 indicate the fractional grating period with high-index and F_2, F_4 indicate the fractional grating period with low-index. Other parameters are the thickness d and period Λ of the grating layer.

The single waveguide grating layer functions as both the diffraction and guiding of light, assuming the structure is transversely infinite.

To attain highly efficient filters, a high spatial frequency grating ($\Lambda < \lambda$) or subwavelength grating is chosen to prevent higher diffraction orders from propagating. This type of structure operates in the zero-order regime, indicating that only zero order diffracted waves propagate with higher orders cutoff. All the materials used in the structures are lossless and free of dispersion, except, as specified. The incident wave is assumed to be a normally-incident TE polarized (the electric field vector is perpendicular to the paper) plane wave.

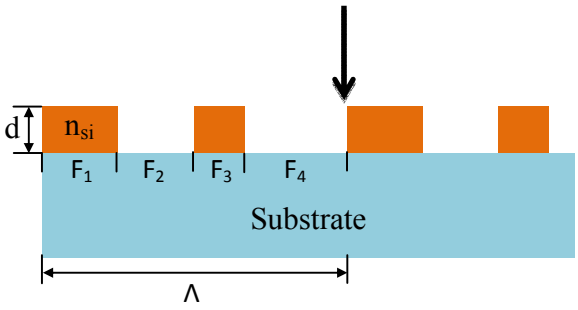

Figure 2.2 Schematic of single-grating-layer GMR structure. Here, Λ and d is the period and thickness of the grating respectively. [F_1, F_2, F_3, F_4] is the filling factor of the grating layer. n_{si} (silicon) is the high-index of grating layer; the low-index of grating layer is assumed to be 1.0 (air). The substrate is usually made of materials like silicon dioxide (SiO_2). The solid black arrow indicates the normally-incident plane wave with TE polarization.

2.3.1.1 Reflection Filter

The first structure treated is a silicon-on-insulator (SOI) single-grating-layer guided-mode resonant (GMR) reflection filter with ~27 nm spectral width. The four-part period grating sits on the silicon dioxide substrate with a refractive index of $n_s = 1.48$. Filling factors are [F_1, F_2, F_3, F_4] = [0.1, 0.13, 0.15, 0.62]; Grating layer thickness and period are d = 0.37 μm and Λ = 0.822 μm, respectively; High-index of grating layer is $n_{si} = 3.48$ and the refractive index of air is

1.0. Figure 2.3 shows the spectral reflectance and phase, time delay and dispersion of a single-layer guided-mode resonant refection filter under a normally incident TE-polarized plane wave. In general, a single-layer resonant leaky mode filter exhibits a spectral phase which changes monotonically by π in the vicinity of the resonance wavelength, as can be seen in Figure 2.3 (b), and a very limited low dispersion band in wavelength in Figure 2.3 (c); appreciable dispersion only occurs at the band edges, shown in Figure 2.3 (d). In Figure 2.3 (a), it is obvious that this single-layer structure has one resonance at the wavelength of 1.569 μm, where it has the largest group delay of 0.226 ps and close to zero dispersion, as shown in Figures 2.3 (c) and (d). Note that the negative time delay means that the peak of reflected wave packet appears at the rear grating plane before the incident wave packet peak reaches the front grating plane.

The maximum delay depends on the linewidth of the reflectance peak for the single resonance structure. This can be interpreted this way: the narrower linewidth of reflectance peak has a larger Q-factor, meaning the electric field will be retarded for a longer time due to resonance. This provides us one feasible way to maximize the time delay by designing resonant nanostructures with proper linewidth of resonance peak. In the following section, one example is given to show that high Q-factor and time delay can be obtained by coupling two identical single-layer leaky-mode resonant reflection filters.

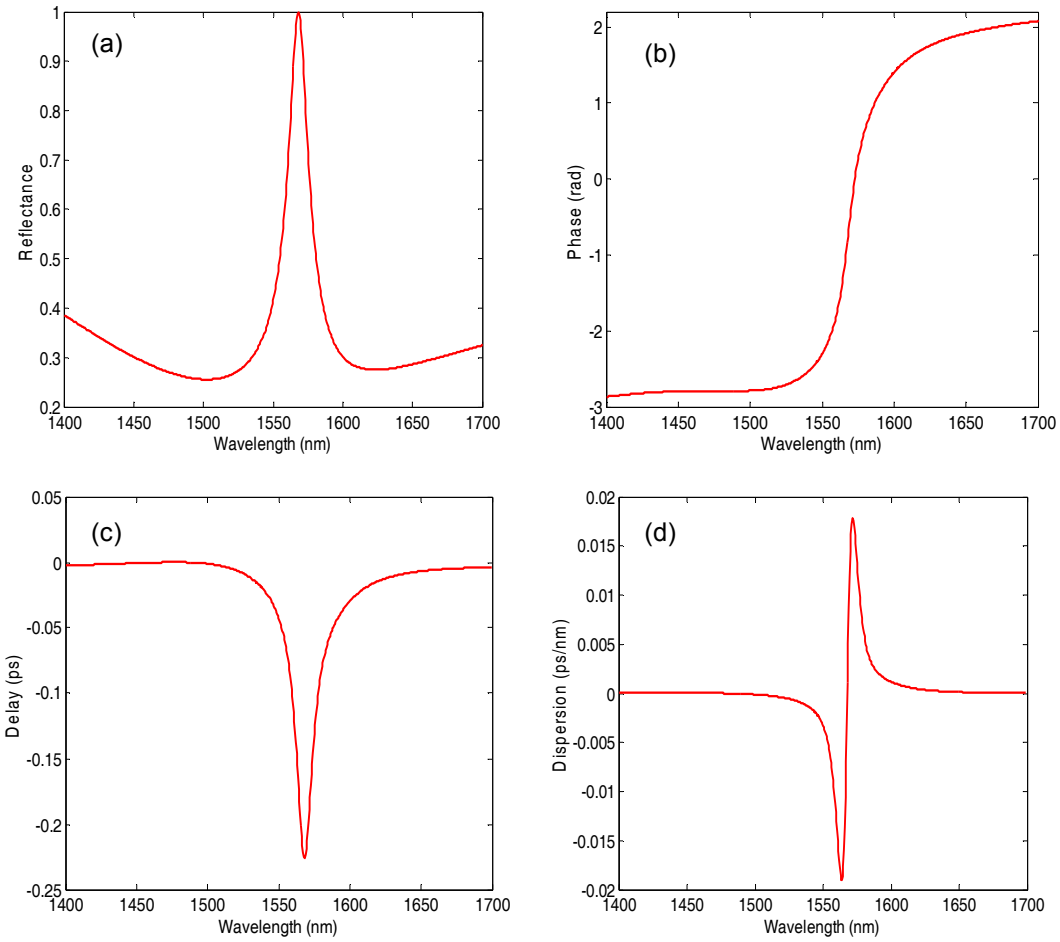

Figures 2.3 (a) Spectral reflectance and (b) phase, (c) time delay and (d) dispersion of the single-grating-layer GMR reflection filter. Structure parameters are [F_1, F_2, F_3, F_4] = [0.1, 0.13, 0.15, 0.62]; d = 0.37 μm; Λ = 0.822 μm; n_{si} = 3.48; n_s = 1.48.

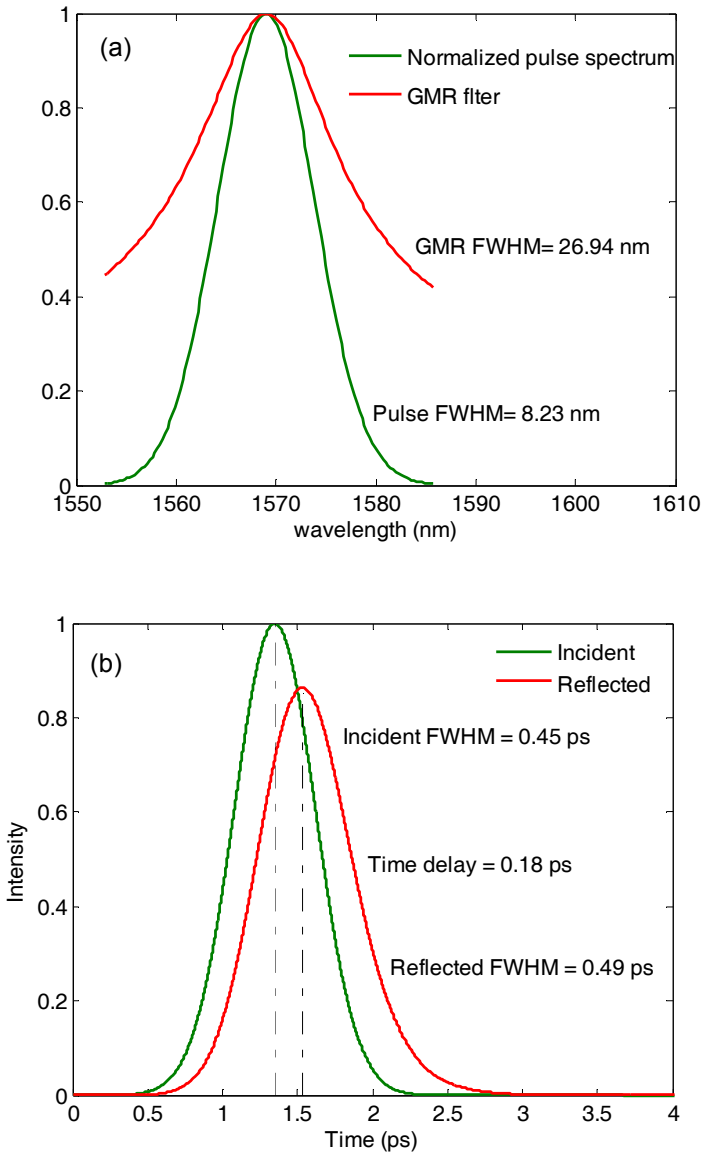

Figure 2.4 (a) The normalized pulse spectrum and GMR reflection filter spectrum; (b) Incident pulse and reflected pulse in time domain.

To verify the time delay, a normalized Gaussian pulse is incident upon the single-layer leaky-mode resonant reflection filter. The reflected pulse and transmitted pulse can be detected and analyzed. Figure 2.4 demonstrates that an optical Gaussian pulse with the central

wavelength of 1.569 μm and temporal full width half maximum (FWHM) width of 0.45 ps, which corresponds to a FWHM width of 8.23 nm in wavelength. The incident pulse experiences a time delay of 0.18 ps. In addition, the maximum intensity of the reflected pulse is reduced to ~86.3% and broadened by ~8.9% in time domain. This is because not all the spectral components of the pulse are within the resonance peak and completely reflected; those outside the resonance peak are partially reflected and suffer the appreciable dispersion, leading to the broadened reflected pulse.

2.3.1.2 Transmission Filter

The second structure is a single-grating-layer silicon-on-insulator (SOI) GMR transmission filter with 0.26 nm spectral width and minimal sidelobes. This filter is designed using the particle swarm optimization (PSO) technique. This device has structural parameters Λ = 979 nm, d = 465 nm, [F_1, F_2, F_3, F_4] = [0.071, 0.275, 0.399, 0.255], n_{si} = 3.48 and n_s = 1.48. Figure 2.5 shows the spectral transmittance and phase response, time delay, and dispersion of this filter under normal incidence with TE polarization. As seen in Figure 2.5 (a), this filter has a transmission resonance at the wavelength of 1524.51 nm. It can provide time delays as high as ~9.6 ps at the transmission resonance, however, the dispersion width is narrow and zero dispersion is obtainable only near 1524.51 nm. Figures 2.6 (a) and (b) display the response of this filter to excitation with a pulse in the spectral (wavelength) and time domains, respectively. The pulse has a full-width half-maximum (FWHM) of 30 ps in time and the central wavelength at 1524.51 nm, and its spectrum fits well spectrally inside the transmission bandwidth of the filter. The output pulse preserves its shape with a delay of ~8.25 ps with respect to the input pulse.

Since this is a leaky-mode resonant transmission filter with a substantial time delay, higher time delay and flat dispersion can be achieved by cascading a large number of such identical transmission filters. In the following sections, examples are shown to verify this approach to attain a desirable time delay.

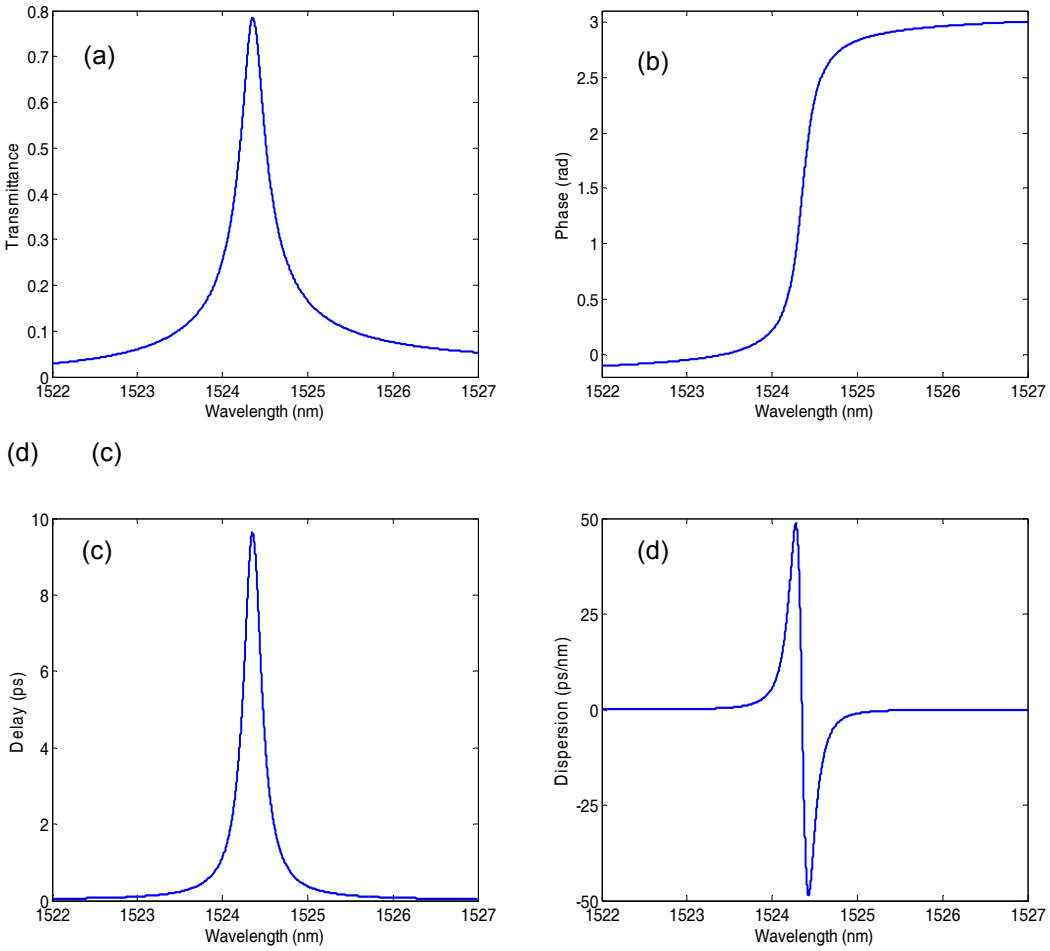

Figures 2.5 (a) Spectral transmittance and (b) phase, (c) time delay and (d) dispersion of the single-grating-layer GMR transmission filter. Structure parameters are: [F_1, F_2, F_3, F_4] = [0.071, 0.275, 0.399, 0.255]; d = 0.465 μm; Λ = 0.979 μm; n_{si} = 3.48; n_s = 1.48.

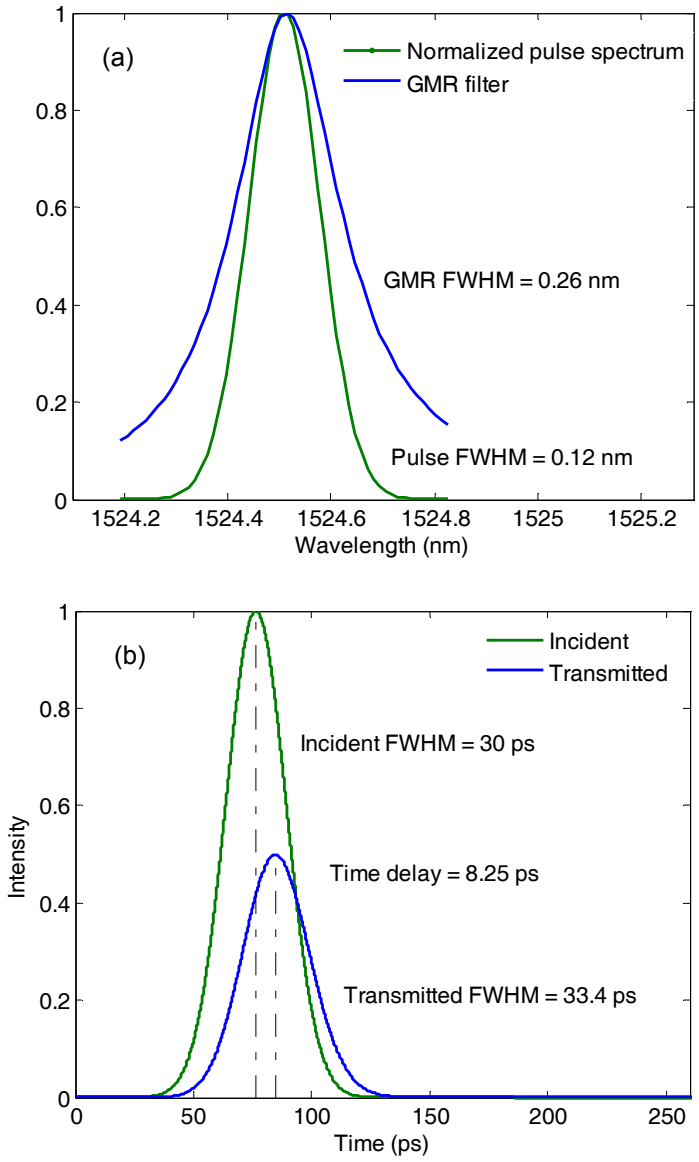

Figure 2.6 (a) The normalized pulse spectrum and GMR transmission filter spectrum (normalized for clear comparison); (b) Incident pulse and transmitted pulse in time domain.

2.3.2 Coupled Single-grating-layer GMR Structures

2.3.2.1 Coupled GMR Reflection Filters

By coupling two identical single-grating-layer GMR reflection filters, novel spectral signatures are realizable. Figure 2.7 shows an example structure. The same GMR reflection filter from section 2.3.1.1 is used to form the coupled GMR reflection filter (note that there is no phase shift or lateral displacement between the two filters). The interference phenomena in a double-sided corrugated waveguide was studied and used to design a narrowband optical filter, where the spatial phase shift between the two corrugated waveguides plays an important role in narrowing the resonance bandwidth [39-40]. Also, by cascading two identical resonant grating reflection filters with sufficiently large gap and π out of phase, increasingly wide and flattened spectral responses were obtained [41]. MEMS tunable resonant leaky mode filters based on the modulation of symmetry profile were also reported; a variable reflector was proposed by vertically tuning the distance between two waveguide gratings [42].

In a coupled GMR reflection filter, a transmission peak (100%) may appear within the range of reflection resonance of the single GMR reflection filter due to the evanescent coupling between the two guides. As the distance between the two reflection filters is tuned, the transmission peak shifts in wavelength. It is possible to design a coupled GMR reflection filter with high Q-factor and time delay. In other words, we can configure the sensitivity of the coupled GMR reflection filters by adjusting the distance between the filters. Figure 2.8 and Figure 2.9 show the transmittance and delay for two different gap distances between the two single-grating-layer GMR reflection filters. It is clear that the width of the transmission peak is much smaller compared with the single GMR reflection filter.

In addition, the width of transmission peak is very sensitive to the gap distance between the two single-grating-layer GMR reflection filters. By changing the gap distance from h = 2.169 μm to h = 2.168 μm, the width of transmission peak is increased from 0.8 pm to 1.3 pm, and the peak delay is reduced from 3.23 ns to 2.01 ns. Figure 2.10 shows the transmittance and delay

for various gap distances. As the distance increase from h = 2.16 μm to h = 2.18 μm, the peak delay first increases and then decrease at the point close to h = 2.17 μm, which is close to the center of reflection resonance of single GMR reflection filter. This can also be explained by the temporal coupled-wave theory as discussed in detail in [43-44].

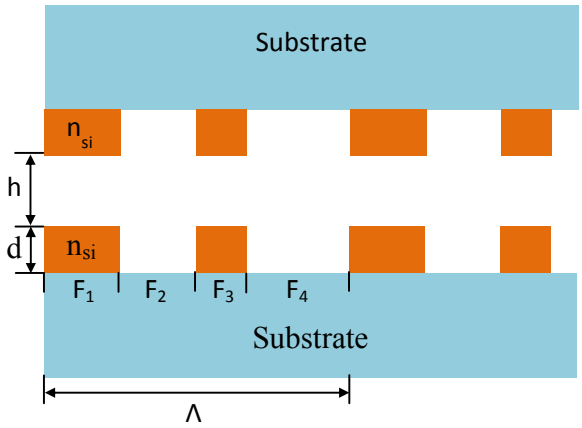

Figure 2.7 Scheme of coupled GMR reflection filters. The gap between the two GMR reflection filters is made of air and h denotes the distance between the two filters. The rest parameters are the same as that in Figure 2.3: [F_1, F_2, F_3, F_4] = [0.1, 0.13, 0.15, 0.62]; d = 0.37 μm; Λ = 0.822 μm; n_{si} = 3.48; n_s = 1.48.

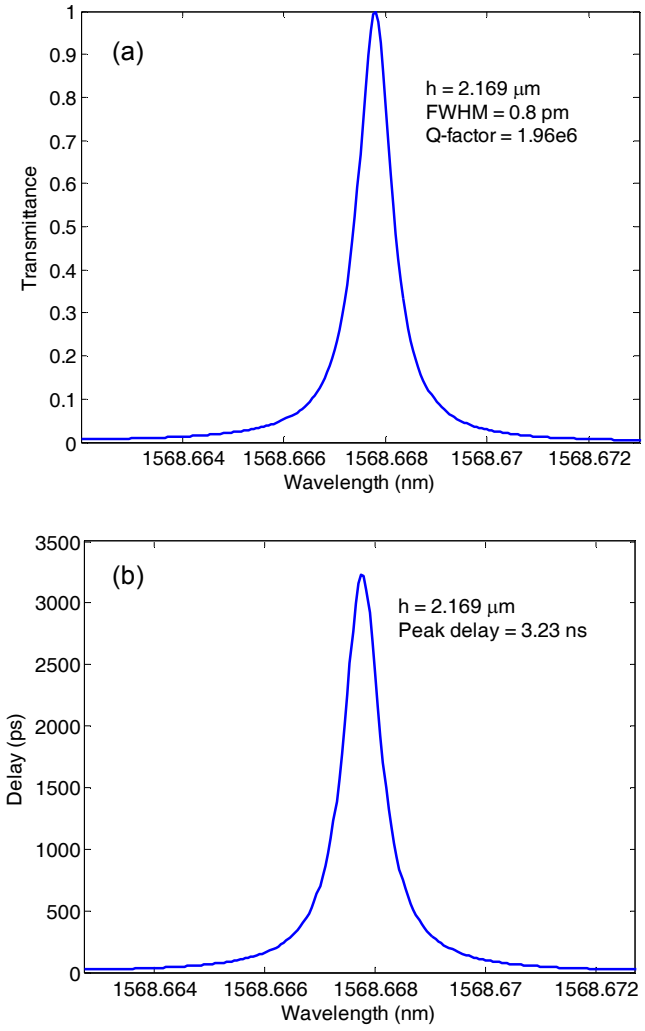

Figure 2.8 Transmittance (a) and delay (b) of a coupled GMR reflection filter with the gap distances of h = 2.169 μm.

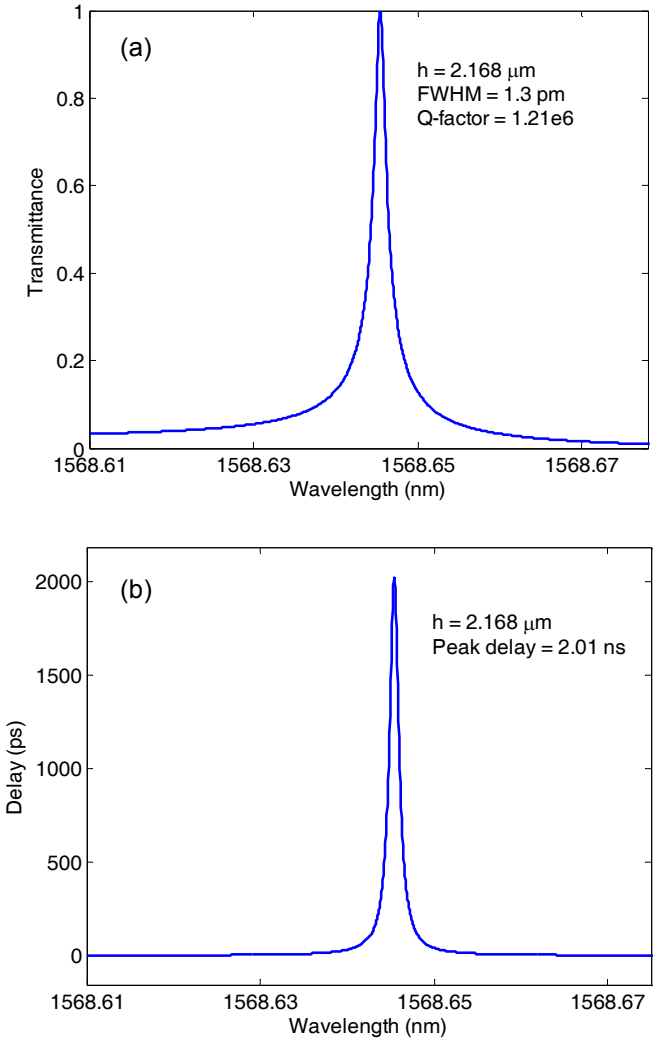

Figure 2.9 Transmittance (a) and delay (b) of a coupled GMR reflection filter with the gap distances of h = 2.168 μm.

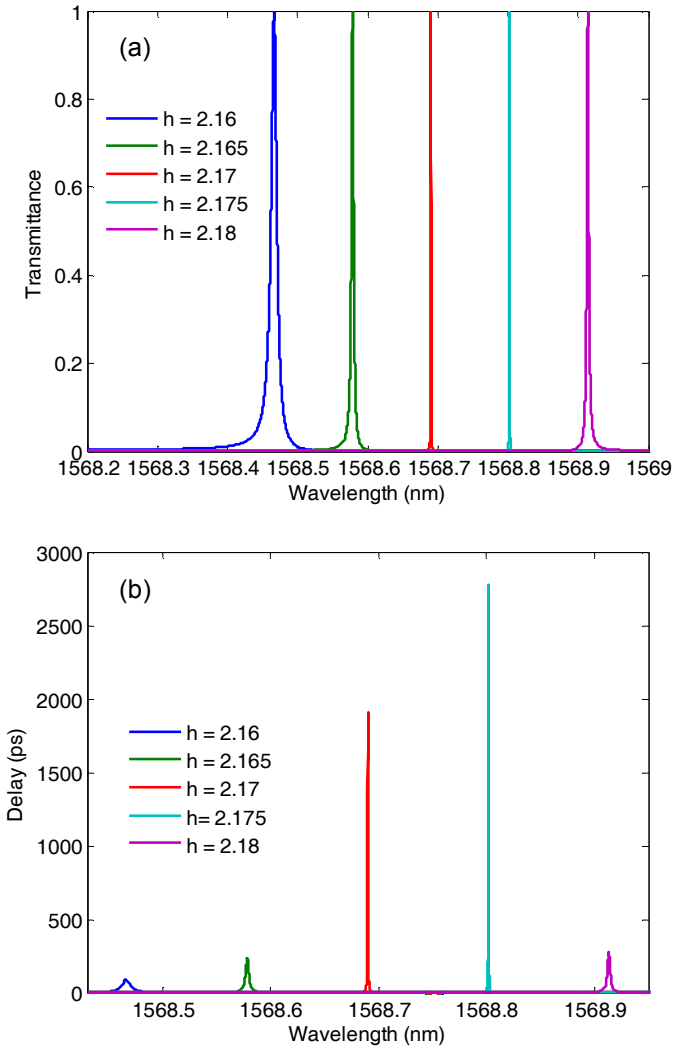

Figure 2.10 Transmittance (a) and delay (b) versus wavelength for various gap distances: h = 2.16 μm, h = 2.165 μm, h = 2.17 μm, h = 2.175 μm, h = 2.18 μm.

2.3.2.2 Cascaded GMR Transmission Filters

Cascading all-pass filter to obtain the desired time delay and dispersion management has been implemented by many researchers, as discussed in Chapter 1. Here, a number of GMR transmission filters are cascaded to realize the desirable time delay and flat dispersion versus wavelength. Figure 2.11 shows the scheme of two cascaded GMR transmission filters

with structure parameters [F_1, F_2, F_3, F_4] = [0.071, 0.275, 0.399, 0.255]; d = 0.465 μm; Λ = 0.979 μm; n_{si} = 3.48. The two cascaded single-grating-layer GMR transmission filters can also be considered as a resonant cavity, and desired time delay is achieved by cascading a number of such cavities [45]. In Figure 2.12, the transmittance, delay and dispersion in wavelength for a cascaded two identical single-grating-layer GMR transmission filters are shown. Compared with the single GMR transmission filter, the FWHM width of the transmission peak is the same (0.5 nm) and the time delay is on the same order. However, the maximum dispersion is reduced from 50 ps/nm to ~13 ps/nm. In the next chapter, it is shown that smaller or even flat dispersion can be achieved by cascading a large number of such cavities formed by two single-grating-layer GMR transmission filters.

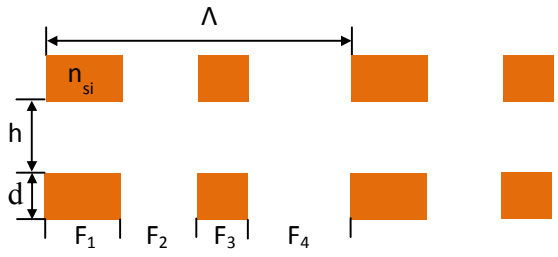

Figure 2.11 Schematic of two cascaded GMR transmission filters. The gap between the two GMR transmission filters is air and h denotes the distance between the two filters. All the rest parameters are: [F_1, F_2, F_3, F_4] = [0.071, 0.275, 0.399, 0.255]; d = 0.465 μm; Λ = 0.979 μm; n_{si} = 3.48.

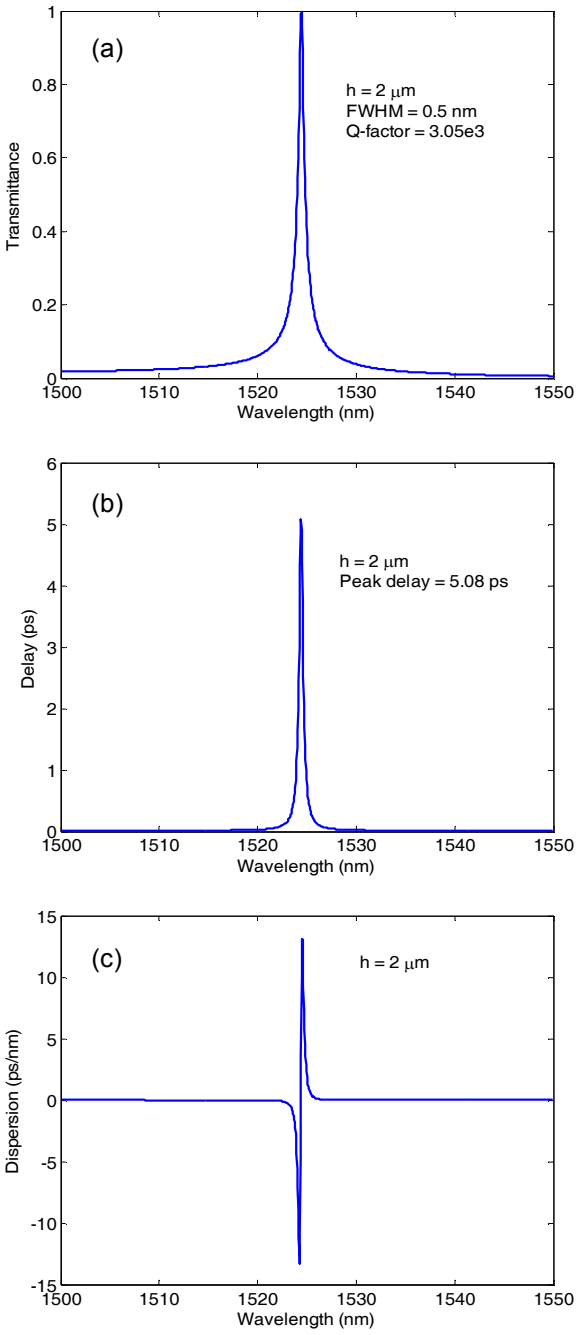

Figure 2.12 Transmittance (a), delay (b) and dispersion (c) from a cascade of two identical single-grating-layer GMR transmission filters with a gap distance of h = 2 μm.

CHAPTER 3

DEVICE APPLICATIONS OF DISPERSION PROPERTIES OF LEAKY-MODE RESONANCE STRUCTURES

3.1 Effect of Loss in Coupled GMR Reflection Filters with High Q-factor

Another limiting factor of optical transmission system is the power loss in waveguides. The power of a light beam travelling through an optical waveguide decreases exponentially due to losses, which arise mainly from absorption and scattering. The attenuation coefficient is defined in units of decibels per kilometer (dB/km) [1] and is denoted here by Γ, which is related to the extinction coefficient k of the waveguide material (the imaginary part of complex refractive index) by the following formula

$$k = \Gamma\lambda/(4\pi), \qquad (3.1)$$

where λ is the wavelength of propagation wave in the waveguide; and Γ is defined by the following equation

$$\Gamma = 10 \log_{10} (P_0/P_L)/L, \qquad (3.2)$$

where the P_L/P_0 is the ratio of transmitted to incident power for a waveguide of length L km. For a light beam propagating through a cascade of several lossy systems, the overall loss in dB is the sum of the dB losses [1].

The attenuation coefficient also depends on wavelength. There are strong absorption bands resulting from various transitions of electrons and molecules in the waveguide. Besides, the randomly localized variations of the molecular may introduce random inhomogeneities in the refractive index, which form scattering centers. The scattered intensity based on this effect is proportional to $1/\lambda^4$, so short wavelengths are scattered more than long wavelengths [1]. However, this thesis mainly considers wavelengths in the transparency window in silicon

waveguides, where scattering is very small. Ignoring scattering losses, the attenuation coefficient is related to propagation loss in 1/μm by the equation

$$\text{Propagation\_}\ \Gamma\ [1/\mu m] = \Gamma\ [dB/km] / (20\times\log_{10}(e)\times 10^{9}). \qquad (3.3)$$

In order to improve the performance of optical waveguides as data-transmission channels, special designs of silicon waveguide including etchless silicon [46], amorphous silicon [47], rib-silicon on insulator [48] and strip-silicon on insulator [49] have been implemented to reduce the propagation loss. Table 3.1 gives a brief summary of typical propagation losses in these designed silicon waveguides. It is acceptable for the optical power travel through a silicon waveguide if the attenuation coefficient is in the range of 0.1-1.6 dB/cm. The coupled GMR reflection filters should be able to survive under such attenuation to be used in practical device applications.

Table 3.1 Reported Losses in Silicon Waveguides

Propagation Loss	**Wavelength**	**Waveguide**
0.3 dB/cm (3.45×10^{-6} μm^{-1})	1.55 μm	Si [46]
0.5 dB/cm (5.76×10^{-6} μm^{-1}) 1.6 dB/cm (1.84×10^{-5} μm^{-1})	1.55 μm 1.30 μm	a-Si [47]
0.1 dB/cm (1.15×10^{-6} μm^{-1})	1.30 μm	rib-Si, SOI [48]
0.92 dB/cm (1.06×10^{-5} μm^{-1})	1.52 μm	strip-Si, SOI [49]

Note: SOI denotes silicon on insulator.

Figure 3.1 gives the transmittance, phase, time delay and dispersion of a coupled GMR reflection filter with an attenuation coefficient $\Gamma = 5\times10^{-6}$ μm^{-1} (0.434 dB/cm). The coupled GMR reflection filter has the same structural parameters as shown in Figure 2.7 except that the substrate is replaced by air. The lossy silicon coupled GMR filter has ~44% peak transmittance and a peak delay of ~3 ns at the resonant wavelength. In Figure 3.2, the transmittance peak reaches ~89% and the peak delay is ~ 6 ns with an attenuation coefficient $\Gamma = 0.5\times10^{-6}$ μm^{-1} (0.0434 dB/cm). By comparing the results of Figure 3.1 and 3.2, it is clear that the attenuation

loss strongly degrades the transmittance and delay. Fortunately, the coupled GMR reflection filters show the potential to be used as a high-Q optical resonator with a high time delay under practical attenuation coefficients.

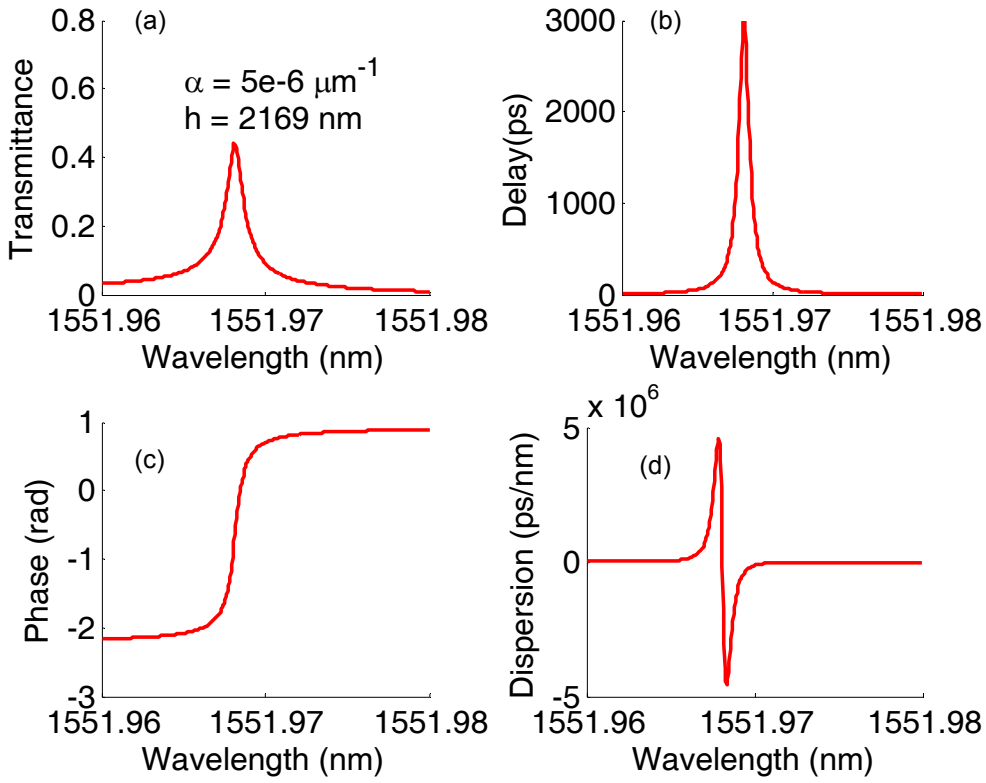

Figure 3.1 Spectral transmittance (a), delay (b), phase (c) and dispersion (d) of a coupled GMR reflection filter with attenuation coefficient $\Gamma = 5 \times 10^{-6}$ μm^{-1} and gap distance h = 2.169 μm. The rest structure parameters are $[F_1, F_2, F_3, F_4] = [0.1, 0.13, 0.15, 0.62]$; d = 0.37 μm; Λ = 0.822 μm; $n_{si} = 3.48$; $n_s = 1.0$ (air).

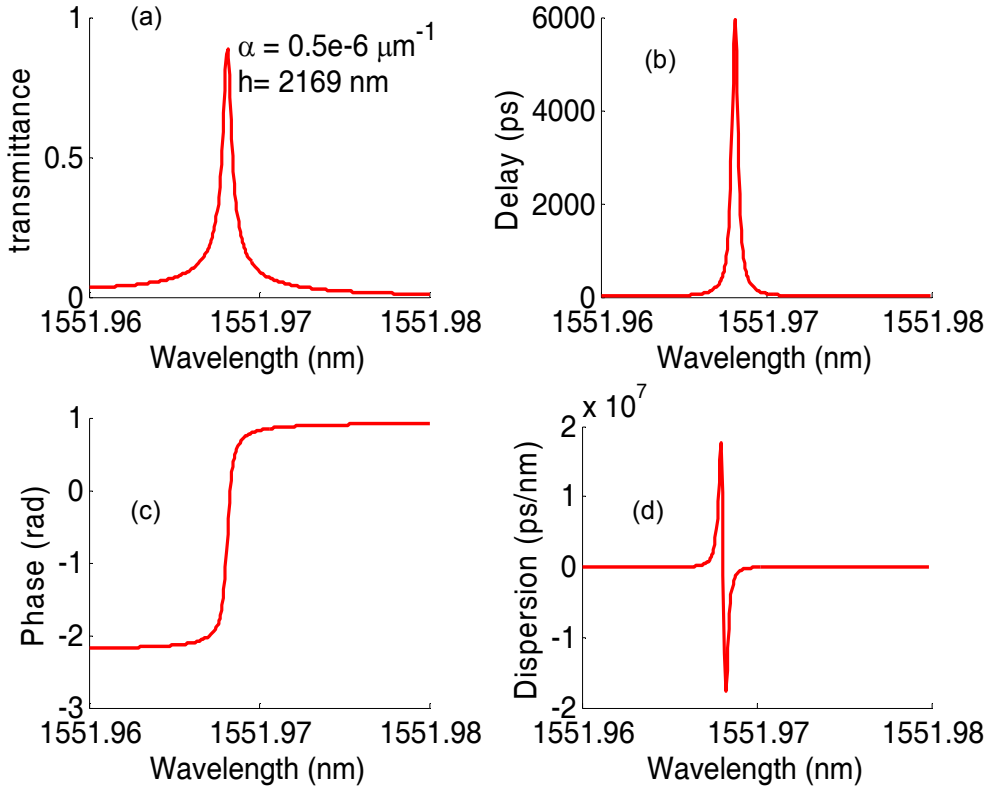

Figure 3.2 Spectral transmittance (a), delay (b), phase (c) and dispersion (d) of a coupled GMR reflection filter with attenuation coefficient $\Gamma = 0.5 \times 10^{-6}$ μm^{-1} and gap distance h = 2.169 μm. The rest structure parameters are $[F_1, F_2, F_3, F_4] = [0.1, 0.13, 0.15, 0.62]$; d = 0.37 μm; Λ = 0.822 μm; $n_{si} = 3.48$; $n_s = 1.0$ (air).

3.2 Cascaded GMR Transmission Filters for DWDM

It is already reported that the cascade of a number of GMR transmission filters can function as a conceptual optical delay lines [45]. And it is known that arrayed waveguide gratings (AWGs) are widely used for dense wavelength division multiplexing (DWDM) applications [50]. AWGs are key devices in the rapidly expanding all-optical DWDM networks, as they integrate multiple optical functions on a single substrate leading to a single package. Cascade of a number of GMR transmission filters can also be employed in DWDM systems with

subnanometric resolution. Figure 3.3 illustrates the cascade of a number of GMR transmission filters with equal gap distance. Along the X direction the structure has a grating periodicity of Λ = 0.979 μm and filling factors of [F_1, F_2, F_3, F_4] = [0.071, 0.275, 0.399, 0.255. Due to the interaction of leaky-mode resonances from each single waveguide layer, multiple transmission peaks may appear in the spectral response of the cascade system of GMR transmission filters.

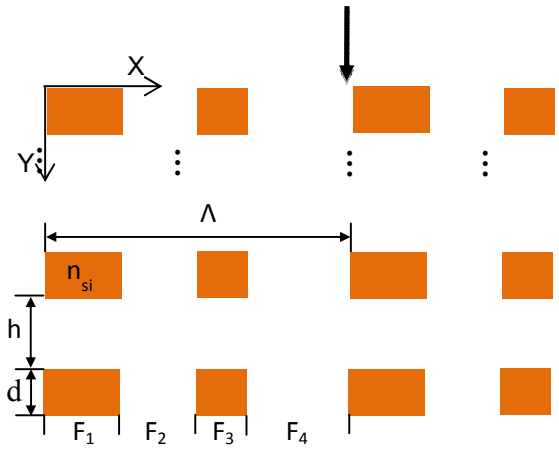

Figure 3.3 Cascade of a number of GMR transmission filters with equal gap distance of h. The single GMR transmission filter has the same structure parameters as those in Figure 2.5 except that the substrate is replaced by air. [F_1, F_2, F_3, F_4] = [0.071, 0.275, 0.399, 0.255]; d = 0.465 μm; Λ = 0.979 μm; n_{si} = 3.48; n_s = 1.0 (air). The solid black arrow indicates the incident plane wave.

Figure 3.4 is an example of cascade of 4 GMR transmission filters. There are three transmission peaks with a spectral FWHM of ~0.2 nm and an equal spacing of ~4 nm in the 1.518 μm -1.53 μm wavelength range, as shown in Figure 3.4 (a). The three transmission channels/peaks have slightly different widths, leading to slightly different peak delays at resonance wavelengths. In a cascade of 7 GMR transmission filters, six channels with the average spacing of 2 nm in 1.518 μm -1.53 μm range are shown in Figure 3.5. The spectral FWHM of each channel is approximately 0.11 nm. 12 channels with a channel spacing of ~ 1 nm (~ 125 GHz in frequency) and the average channel bandwidth of 0.05 nm are observed in

the 1.518 μm -1.53 μm band at the spectral response of a cascade of 13 GMR transmission filters, as shown in Figure 3.6.

The wavelength range is primarily determined by the gap distance between the two neighboring GMR transmission filters. The average linewidth of these transmission peaks (or average bandwidth of channels) gets smaller and thus higher time delay and dispersion in Figure 3.5, compared with the computed results in Figure 3.4. Generally, N channels can be obtained by cascading (N+1) GMR transmission filters, which create N cavities. And the corresponding channel bandwidth and the spacing between two neighboring channels both get smaller with the increasing number of cascaded GMR transmission filters. In addition, the spacing and channel bandwidth can be tuned by adjusting the structure parameters such as the thickness and period of grating layer, filling factors and refractive index.

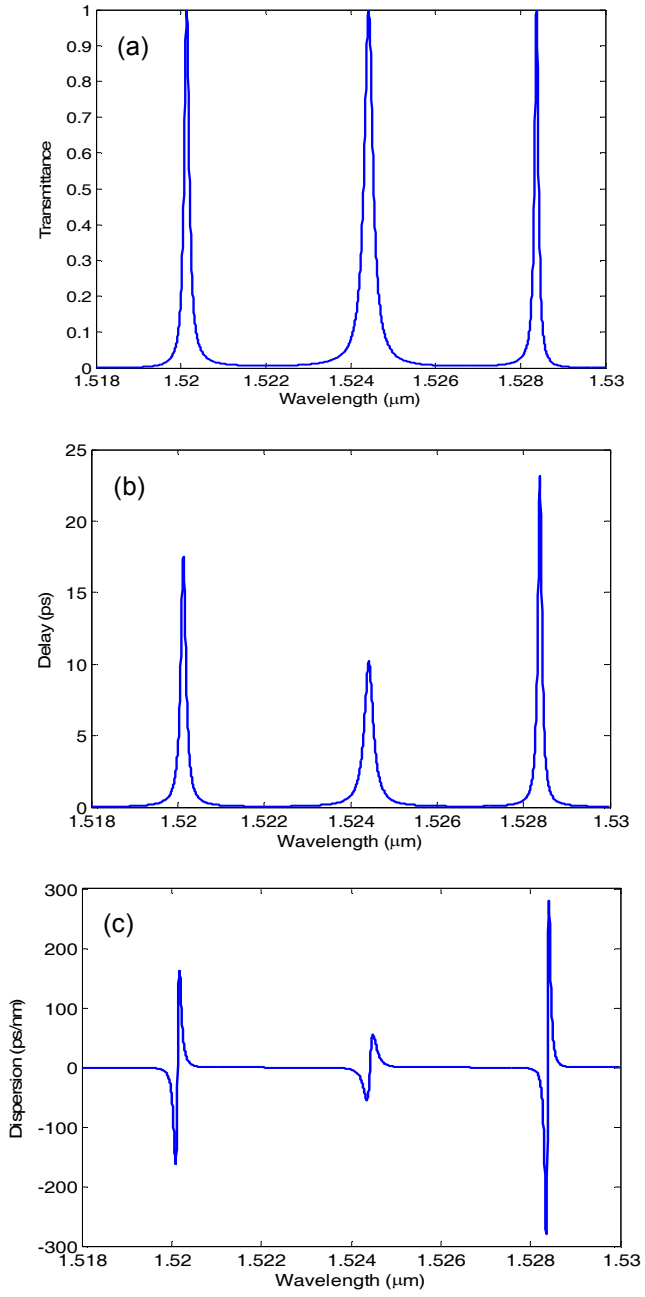

Figure 3.4 Spectral response (a), time delay (b) and dispersion (c) of a cascade of 4 GMR transmission filters with gap distance h = 2 μm.

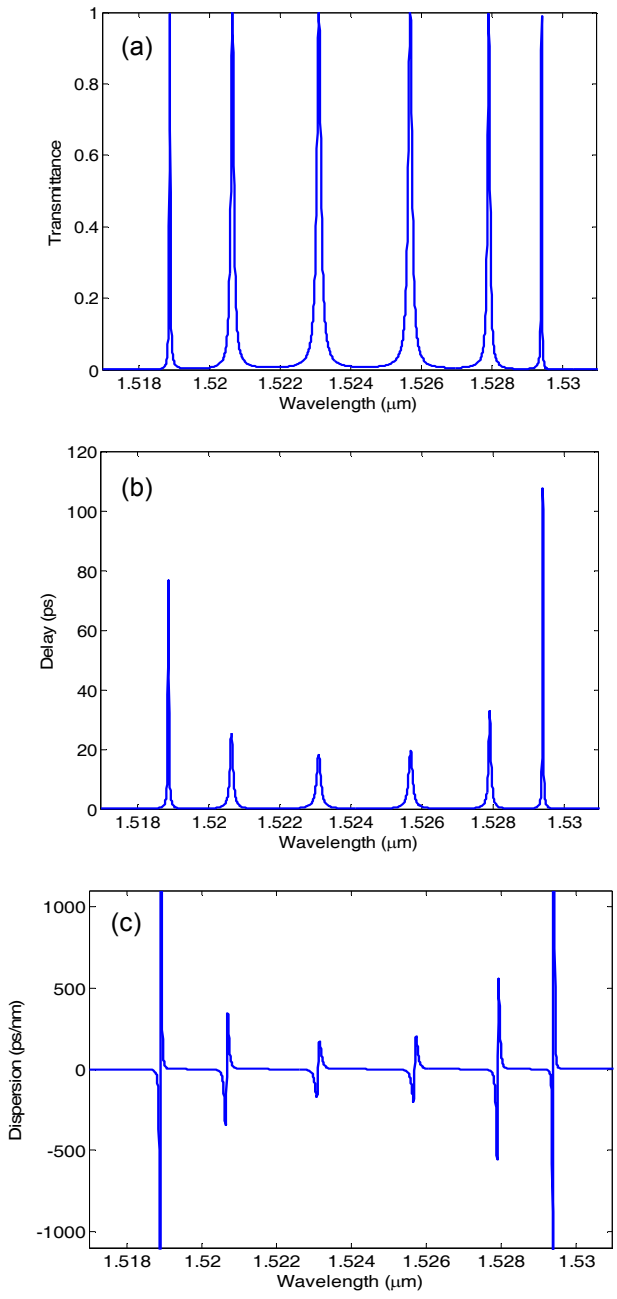

Figure 3.5 Spectral response (a), time delay (b) and dispersion (c) of a cascade of 7 GMR transmission filters with gap distance h = 2 μm.

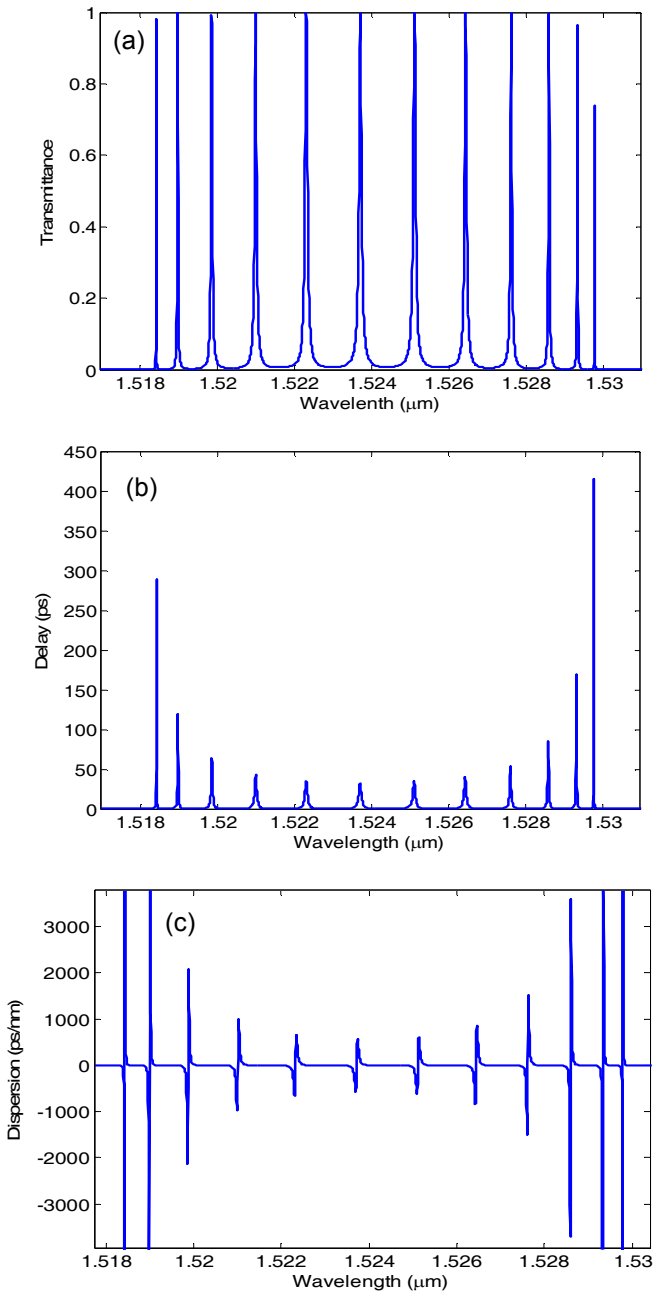

Figure 3.6 Spectral response (a), time delay (b) and dispersion (c) of a cascade of 13 GMR transmission filters with gap distance h = 2 μm.

3.3 Slow Light and Optical Delay Lines

Two free-standing membranes (single-grating-layer GMR transmission filter) with an air gap (cavity) between them is used to realize a ~0.75 nm (FWHM) flat-top transmission band as shown in Figure 3.7. Again, this structure is designed by PSO and its structural parameters are: Λ = 1103.9 nm, d = 432.2 nm, [F1, F2, F3, F4] = [0.0626, 0.3013, 0.4576, 0.1785], and d_C = 2000 nm (the cavity width). Figure 3.7 illustrates the transmittance, phase, delay, and dispersion of this single cavity device. This element shows a flat-top transmission bandwidth, which actually is a result of merging two adjacent narrow transmission resonances. In addition, the delay response exhibits an average of ~7 ps in the transmission band. Figure 3.8 shows the pulse response of this filter in wavelength and time domains, respectively. The input pulse has a FWHM of 20 ps in time and spectrally fits well inside the transmission bandwidth of the filter. The input pulse is delayed by ~6.1 ps by being transmitted through this filter in good agreement with the delay in Figure 3.7.

By cascading the single-cavity filter as that in Figures 3.7, we can build a structure resembling a multi-cavity photonic crystal waveguide [51]. To illustrate, we cascade five GMR subunits with spacing d_B= 5.0 μm (the distance between two neighboring cavities). Figure 3.9 shows the computed results. Although the high-transmission bandwidth is smaller than it is for the single-cavity structure, cascading the cells results in a flat delay response of ~30 ps over a ~0.5 nm wavelength band. Moreover, the flat low-dispersion response illustrates that such structures are promising for imposing constant (and almost dispersion-free) delays on optical pulses. Theoretically, this ~30 ps group delay for the ~34 μm long structure designed here corresponds to a group velocity of ~0.0038c_0. Figure 3.10 displays the response of this filter to pulse excitation. The input pulse has a temporal FWHM of 30 ps, and the output pulse preserves its shape with a delay of ~30 ps with respect to the input pulse. For comparison, Notomi et al. reported 75 ps delay with 60 cavities each being 2100 nm in diameter; the total structure length was 175 mm [51].

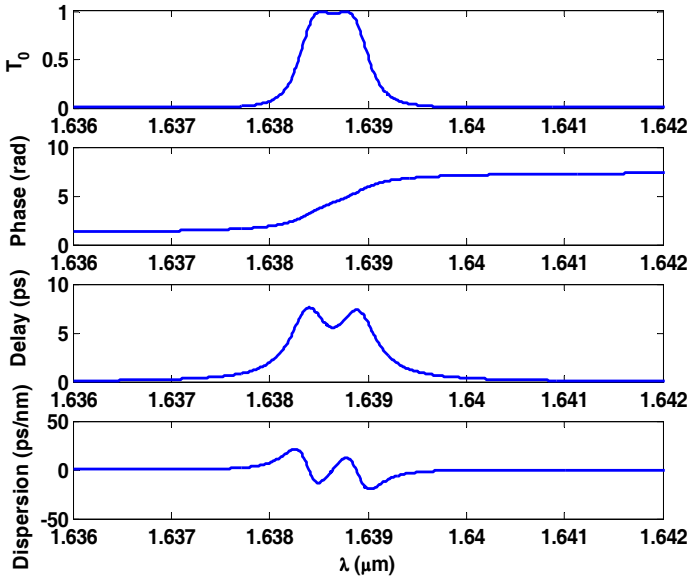

Figure 3.7 Spectral transmittance (T_0) and phase, time delay and dispersion of single-cavity filter. Λ=1103.9 nm, d = 432.2 nm, [F1, F2, F3, F4] = [0.0626, 0.3013, 0.4576, 0.1785], and d_C = 2000 nm.

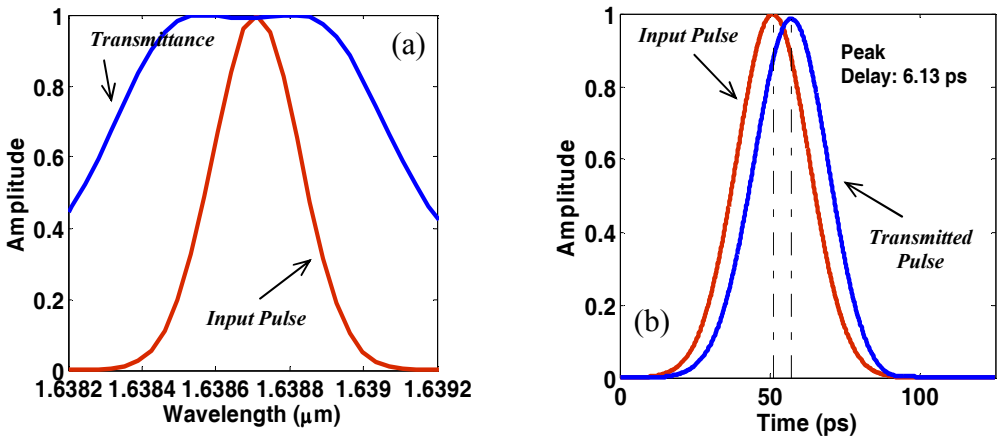

Figure 3.8 Pulse response of the single-cavity filter. (a) Spectrum of the input pulse in relation to the filter spectrum. (b) Time domain response. FWHM of the input pulse is 20 ps.

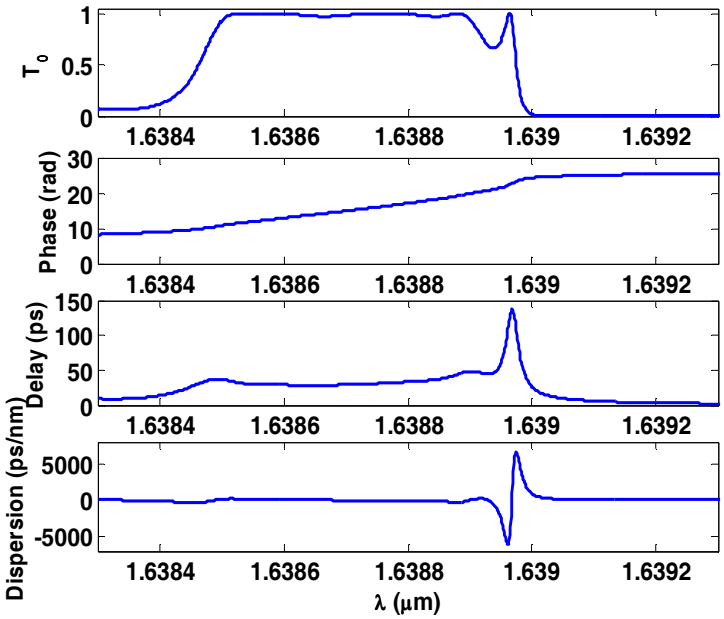

Figure 3.9 Spectral transmittance (T_0) and phase, delay and dispersion of the five-cavity GMR transmission filter. Λ=1103.9 nm, d = 432.2 nm, [F1, F2, F3, F4] = [0.0626, 0.3013, 0.4576, 0.1785], d_C = 2000 nm, d_B = 5000 nm.

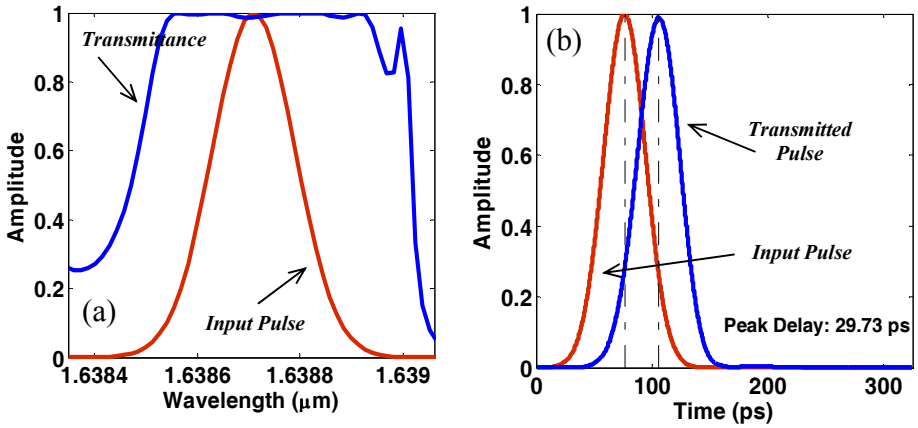

Figure 3.10 Pulse response of this filter (a) in wavelength, and (b) in time domain. The output pulse experiences a ~30 ps time delay with respect to the input pulse.

Figure 3.11 shows a conceptual implementation of a GMR slow-light device. If the device height d_D is large, the device functions as a bulk element. Each sub-ridge layer is a GMR element like in Figure 2.11. If we design the sublayer to operate as a bandpass filter, the input

light will resonate transversely and be reradiated forward to the next GMR layer. This idea can also be implemented with a series of GMR filters on numerous substrates cascaded as a stack. The concept in Figure 3.11 is convenient in that a large number of cascaded resonant units can be fabricated in a few steps by e-beam lithography (EBL) and deep reactive ion etching (DRIE), resulting in a compact system of resonant delay units. Certainly, the dimensions of the device and the input beam size should be specified with practical limitations in mind. On the other hand, if thickness d_D is small, such as on the order of 100-300 nm, this can be a waveguide device. In that case, the functionality of the device employs waveguiding is a dual sense. First, there is the waveguide that guides light from one resonant layer to the next. For that to work, the structure requires a higher average refractive index than that of the surrounding media as usual. A membrane in air will satisfy this requirement with additional considerations if the device sits on a substrate. Second, each GMR cell forms a resonant waveguide. In principle, we can cascade a large number of these GMR cells to achieve a specified time delay. Indeed, multiple-cell cascading is the basis for the new coupled-resonator optical waveguide (CROW) technology being developed [51].

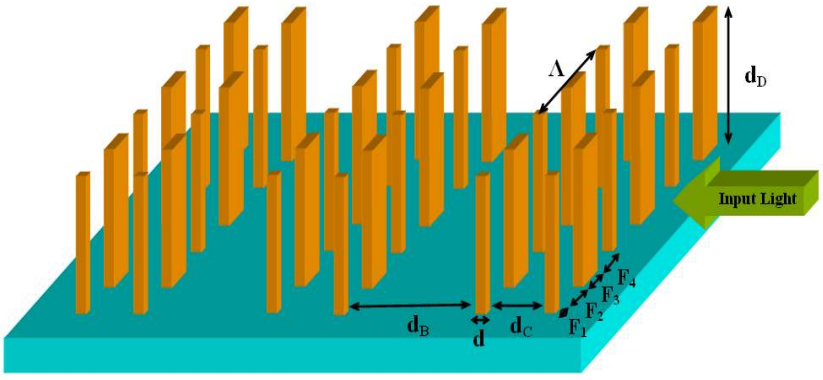

Figure 3.11 Schematic view of a conceptual implementation of an example GMR slow-light device. Multiple resonant units can be cascaded to realize a specified delay. Only three subunits, each based on two transversely-resonant GMR elements, are shown. Here, d_D is the device thickness, d_C is the cavity length, and d_B is the buffer length. Other parameters are defined in Figure 2.11 [45].

CHAPTER 4

CONCLUSIONS

4.1 Contributions

In the past, considerable research work has been performed on the spectral amplitude properties of leaky-mode resonance structures. In contrast, the spectral phase properties which are directly related to the dispersive properties have received less attention. In this thesis, a numerical computation method for the analysis of optical pulses propagating through leaky-mode/guided-mode resonance structures is formalized and implemented based on the combination of Fourier spectral decomposition technique and rigorous coupled-wave analysis (RCWA) method. Then, the dispersion properties of various leaky-mode resonance example structures including single-grating-layer GMR reflection and transmission filters, cascaded GMR filters, and coupled GMR filters are analyzed numerically in details. Specifically, the phase, time delay and dispersion characteristics of each device are studied, as well as their interaction with optical pulses. Finally, device applications such as high-Q filter, DWDM filter, and optical delay lines based on the dispersion properties of leaky-mode resonance structures are proposed. High-Q transmission filter can be designed from a coupled narrow linewidth GMR reflection filters. The loss analysis shows that this high-Q property can withstand typical attenuation losses in silicon waveguides. By cascading a number of GMR transmission filters, dense wavelength division multiplexing filters with subnanometric resolution are proposed. DWDM filter with N channels can be made from a cascade of N+1 GMR transmission

filters. The channel bandwidth strongly depends on the gap distance between two neighboring GMR transmission filters. A conceptual implementation of GMR optical delay line device is also proposed.

4.2 Future Work

All the contributions in the thesis are limited in three aspects. Firstly, leaky-mode structures are TE-polarized and the incident pulse is TE-polarized incident Gaussian pulse. Future work can be performed in TM-polarized cases. Secondly, all the leaky-mode structures are one-dimensional structures or mixture of one-dimensional structures. Future work can be done for two-dimensional cases. Thirdly, all the presented results need to be verified by physical experiments. Future work on the experiment setup to verify the time delay and dispersion properties of such devices is necessary. In addition, to implement a practical device, the imperfection and perturbation during fabrication of such devices also need to be considered, which is out of the scope of the thesis. In addition, these proposed devices can be optimized by using various optimization and design methods.

REFERENCES

[1] B. E. A. Saleh, M. C. Teich, FUNDAMENTALS OF PHOTONICS, 2nd edition, A John Wiley & sons, Inc., Publication, Chapter 9, 2009

[2] G. P. Agrawal, Fiber-Optic Communication Systems, Wiley, New York, 1992

[3] A. J. Antos and D. K. Smith, “Design and characterization of dispersion compensating fiber based on the LP01 mode,” J. Lightwave Technol. 12, 1739-1745, 1994

[4] F. Ouellette, “Dispersion cancellation using linearly chirped Bragg grating filters in optical waveguides,” Opt. Lett., Vol. 12, No. 10, 847-849, 1987

[5] D. Mendlovic, z. Zalevsky, and P. Andreas, “A novel device for achieving negative or positive dispersion and its applications,” Optik (Stuttgart) 110, 45-50, 1999

[6] C. K. Madsen and G. Lenz, “Optical all-pass filters for phase response design with applications for dispersion compensation,” IEEE Photonics Technol. Lett. 10, 994-996, 1998

[7] G. Lenz and C. K. Madsen, “General optical all-pass filter structures for dispersion control,” J. Lightwave Technol. 17, 1248-1254, 1999

[8] C. K. Madsen, G. Lenz, A. J. Bruce, M. A. Cappuzzo, L. T. Gomez, and R. E. Scotti, “Integrated all-pass filters for tunable dispersion and dispersion slope compensation,” IEEE Photonics Technol. Lett. 11, 1623-1625, 1999

[9] I. Kaminow and T. Li, Optical Fiber Telecommunications IV, 4th edition, Academic, San Diego, CA, Part B, 642-724, 2002

[10] P. Vincent and M. Neviere, “Corrugated dielectric waveguides: A numerical study of the second-order stop bands,” Appl. Phys. 20, 345-351, 1979

[11] L. Mashev and E. Popov, “Zero order anomaly of dielectric coated gratings,” Opt. Comm. 55, 377-380, 1985

[12] E. Popov, L. Mashev, and D. Maystre, “Theoretical study of anomalies of coated dielectric gratings,” Opt. Acta 33, 607–619, 1986

[13] G. A. Golubenko, A. S. Svakhin, V. A. Sychugov, and A. V. Tishchenko, “Total reflection of light from a corrugated surface of a dielectric waveguide,” Sov. J. Quantum Electron. 15, 886-887, 1985

[14] I. A. Avrutsky and V. A. Sychugov, “Reflection of a beam of finite size from a corrugated waveguide,” J. Mod. Opt. 36, 1527-1539, 1989

[15] R. Magnusson and S. S. Wang, “New principle for optical filters,” Appl. Phys. Lett. 61, 1022-1024, 1992

[16] S. S. Wang and R. Magnusson, “Theory and applications of guided-mode resonance filters,” Appl. Opt. 32, 2606-2613, 1993

[17] S. M. Norton, T. Erdogan and G. M. Morris, “Coupled-mode theory of resonant-grating filters,” J. Opt. Soc. Am. A 14, 629-639, 1997

[18] T. Tamir and S. Zhang, “Resonant scattering by multilayered dielectric gratings,” J. Opt. Soc. Am. A 14, 1607-1616, 1997

[19] Y. Ding and R. Magnusson, “Resonant leaky-mode spectral-band engineering and device applications,” Opt. Express 12, 5661-5674, 2004

[20] Y. Ding and R. Magnusson, “Use of nondegenerate resonant leaky modes to fashion diverse optical spectra,” Opt. Express, 12, 1885-1891, 2004

[21] S. S. Wang and R. Magnusson, “Design of waveguide-grating filters with symmetrical line shapes and low sidebands”, Opt. Lett. 19, 919-921, 1994

[22] M. Shokooh-Saremi and R. Magnusson, “Wideband leaky-mode resonance reflectors: Influence of grating profile and sublayers,” Opt. Express 16, 18249-18263, 2008

[23] Y. Ding and R. Magnusson, “Band gaps and leaky-wave effects in resonant photonic-crystal waveguides,” Opt. Express 15, 680-694, 2007

[24] F. Schreier, M. Schmitz and O. Bryngdahl, “Pulse delay at diffractive structures under resonance conditions,” OPTICS LETTERS, Vol. 23, No. 17, 1337-1339, 1998

[25] F. Schreier and O. Bryngdahl, “Confined wave packets in the domain of Rayleigh-Wood anomalies,” J. Opt. Soc. Am. A, vol. 17, No. 1, 68-73, 2000

[26] S. Tibuleac and R. Magnusson, “Reflection and transmission guided-mode resonance filters,” J. Opt. Soc. Am. A 14, 1617-1626, 1997

[27] M. S. Mirotznik, D. W. Prather, J. N. Mait, W. A. Beck, S. Shi and X. Gao, “Three-dimensional analysis of subwavelength diffractive optical elements with the finite-difference time-domain method,” APPLIED OPTICS, Vol. 39, No. 17, 2878-2879, 2000

[28] W. Suh and S. Fan, "All-pass transmission or flattop reflection filters using a single photonic crystal slab," Appl. Phys. Lett. 84, 4905-4907, 2004

[29] W. Nakagawa, R. Tyan, P. Sun, F. Xu and Y. Fainman, “Ultrashort pulse propagation in near-field periodic diffractive structures by use of rigorous coupled-wave analysis,” J. Opt. Soc. Am. A, Vol. 18, No. 5, 1072-1081, 2001

[30] T. Vallius, P. Vahimaa and J. Turunen, “Pulse Deformations at guided-mode resonance filters,” OPTICS EXPRESS, Vol. 10, No. 16, 840-843, 2002

[31] H. Ichikawa, “Electromagnetic analysis of diffraction gratings by the finite-difference time-domain method,” J. Opt. Soc. Am. A, Vol. 15, No. 1, 152-157, 1998

[32] H. Ichikawa, “Analysis of femtosecond-order optical pulses diffracted by periodic structure,” J. Opt. Soc. Am. A, Vol. 16, No. 2, 299-304, 1999

[33] T. Erdogan,”Fiber grating spectra,” J. Lightwave Technol., Vol. 15, No. 8, 1277-1293, 1997

[34] C. Wang, L. Liu, A. Yan, D. Liu, D. Li, and W. Qu, “Pulse shaping properties of volume holographic gratings in anisotropic media,” J. Opt. Soc. Am. A, Vol. 23, No. 12, 3191-3196, 2006

[35] M. G. Moharam and T. K. Gaylord, “Diffraction analysis of dielectric surface relief gratings,” J. Opt. Soc. Am. 72, 1385-1392, 1982

[36] T. K. Gaylord and M. G. Moharam, “Analysis and applications of optical diffraction by gratings,” Proc. IEEE 73, 894-937, 1985

[37] R. Eberhart and J. Kennedy, “Particle swarm optimization,” in Proceedings of IEEE Conference on Neural Networks (IEEE, 1995), 1942-1948

[38] M. Shokooh-Saremi and R. Magnusson, “Particle swarm optimization and its application to the design of diffraction grating filters,” Opt. Lett. 32, 894-896, 2007

[39] I. A. Avrutsky, A. S. Svakhin and V. A. Sychugov, “Interference phenomena in waveguides with two corrugated boundaries,” J. of Modern Optics 36, 1303-1320, 1989

[40] B. A. Usievich, V. A. Sychugov and D. K. Nurligareev, “Narrowband optical filter based on a Fabry-Perot interferometer with two waveguide-grating mirrors,” Quantum Electron. 37, 475-478, 2007

[41] D. K. Jacob, S. C. Dunn and M. G. Moharam, “Flat-top narrow-band spectral response obtained from cascaded resonant grating reflection filters,” Appl. Opt. 41, 1241-1245, 2002

[42] R. Magnusson and Y. Ding, “MEMS tunable resonant leaky mode filters,” IEEE Photonics Technol. Lett. 18, 1479-1481, 2006

[43] H. Y. Song, S. Kim and R. Magnusson, “Tunable guided-mode resonances in coupled gratings,” OPTICS EXPRESS, Vol. 17, No. 26, 23544-23555, 2009

[44] J. D. Joannopoulos, R. D. Meade, and J. N. Winn, *Photonic Crystals: Molding the Flow of Light*, Princeton, 1995

[45] R. Magnusson, M. Shokooh-Saremi, and X. Wang, “Dispersion engineering with leaky-mode resonant photonic lattices,” OPTICS EXPRESS, Vol. 18, No. 1, 108-116, 2010

[46] J. Cardenas, C. B. Poitras, J. T. Robinson, K. Preston, L. Chen, and M. Lipson, “Low loss etchless silicon photonic waveguides,” OPTICS EXPRESS, Vol. 17, No. 6, 2009

[47] A. Harke, M. Krause, and J. Mueller, “Low-loss single-mode amorphous silicon waveguides”, ELECTRONICS LETTERS, Vol. 41 No. 25, 2005

[48] U. Fischer, T. Zinke, J. R. Kropp, F. Arndt, and K. Petermann, “0.1 dB/cm Waveguide Losses in Single-Mode SOI Rib Waveguides,” IEEE Photon. Technol. Lett. 8, 1996

[49] M. Gnan, S. Thoms, D. S. Macintyre, R. M. De La Rue and M. Sorel, “Fabrication of low-loss photonic wires in silicon-on-insulator using hydrogen silsesquioxane electron-beam resist,” Electron. Lett. 44, 2008

[50] H Takahashi, S Suzuki, K Kato, and I Nishi, “Arrayed-waveguide grating for wavelength division multi/demultiplexer with nanometer resolution,” Electronics Lett. 26, 87-88, 1990

[51] M. Notomi, E. Kuramochi, and T. Tanabe, “Large-scale arrays of ultrahigh-Q coupled nanocavities,” Nature Photon. 2, 741-747, 2008

BIOGRAPHICAL INFORMATION

Xin Wang received his Bachelor of Science degree in Electronics Science and Technology from Harbin Institute of Technology, China in 2007. Since 2008, he has been a graduate research assistant in the department of Electrical Engineering at The University of Texas at Arlington, studying diffractive and waveguide optics, guided-mode/leaky-mode resonance phenomena in periodic structures, and applications in dispersion engineering. He has also developed a Labview feedback control to stabilize the interference pattern for a UV holographic lithography system at the University of Connecticut in 2007. His research interests include, but not limited to, diffractive optics, waveguide optics, silicon photonics, integrated photonics, slow light techniques, bio-sensing etc. After the graduation with a Master of Science degree in Electrical Engineering from the University of Texas at Arlington, he plans to pursue a PhD degree in optics and photonics area. He is a member of the Optical Society of America and a member of the Golden Key International Honor Society — UTA chapter.